International Forum on Aeroelasticity and Structural Dynamics
IFASD 2024
17-21 June 2024, The Hague, The Netherlands

FLUTTER AND GUST RESPONSE OF A WING WITH AERODYNAMIC GAPS

Dale M. Pitt

Dale M. Pitt Engineering LLC

Keywords: flutter, gust, aerodynamic gap, box pressure modifications, ZAERO, static lift and moment, Doublet Lattice Method (DLM)

Abstract: Recent research on the effects of spanwise and streamwise aerodynamic gaps incorporated in a simple swept wing is presented. The wing flutter and gust response is systematically investigated for a series of aerodynamic gaps. This paper presents the results of a systematic approach to modeling aerodynamic gaps in both the spanwise and streamwise directions of a simple swept wing. Forty different chordwise aerodynamic gaps and forty different spanwise gaps were examined. A process was employed that utilized ZAERO to zero the box pressures that simulate the aerodynamic gap. This process involved a MATLAB script to zero the pressures of the wing boxes that were in turn inputted to ZAERO for flutter and gust analysis. Lastly, the wing locations for maximum increase in the flutter speed and maximum decrease in wing root bending, root shear and root bending moment are presented.

1 INTRODUCTION

Pendelton, Lee and Waserman [1] report the design, fabrication, analyses, and wind tunnel test of a low speed flexible model that simulated an F-16 derivative wing design. The aeroelastic model was equipped with multiple leading and trailing edge control surfaces. The results of the wind tunnel test demonstrated the advantage of using Active Flexible Wing technology. The model was constructed of a single aluminum beam to represent the EI and GJ of the Elastic Axis. The wing airfoil was represented by Balsa Wood segments that were fastened to the aluminum spar and separated by small physical gaps between the aerodynamic sections that were designed to not change the beam EI and GJ characteristics as the wing model deflected and twisted. It was found that the unsealed aerodynamic gaps significantly changed the model measured wing bending moment. Sealing the air gaps with tape increased the wing bending moment but also increased stiffness and damping. Figure 1 is reproduced from reference [1]. The left side of the figure depicts the wind tunnel model planform and the locations of all the aerodynamic gaps. The right side of the Figure [1] displays the improvement in the wind bending moment upon sealing the aerodynamic between leading edge flap and the main wing torque box.

Around this same time, McDonnell Aircraft tested a low-speed flutter model of the F/A-18E/F with similar construction of a wing beam representing the wing stiffness and mass properties. The flutter model also had balsa aerodynamic wing sections located spanwise on the beam. The flutter model was constructed with small phjysica gaps between the airfoil sections. This was designed to have minimal change on the wing stiffness. The F/A-18 E/F measured low-speed

wind tunnel flutter model velocities were slightly higher than those calculated using Doublet Lattice Method, upon sealing the gaps with latex sheet the flutter speeds were reduced and matched the flutter analysis better.

2 PRESENT INVESTIGATION

It was decided to investigate the effects of streamwise (chordwise variation) and spanwise aerodynamic gaps (constant chord locations) on flutter and gust response using current industry analysis techniques. A simple swept wing plate model was used in this investigation.

2.1.1 Literature Review

A literature review reveals that the previous primary interest in wing aerodynamic gaps has been on the vehicle aerodynamic performance due to physical gaps on the lifting surface.

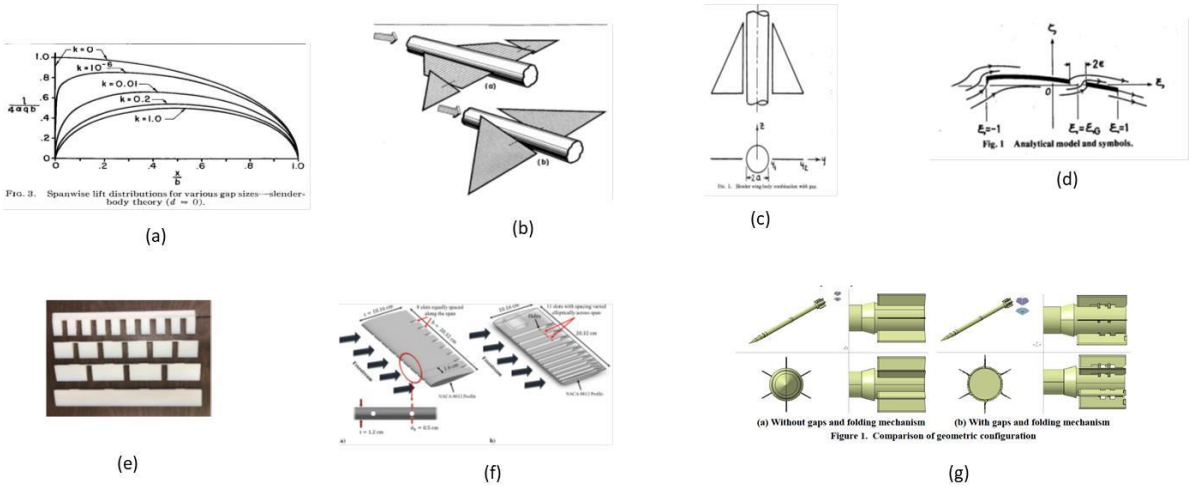

Figure 2. Examples of Aerodynamic Gaps in the Literature

Some of the earliest research [2, 3, and 4] investigated gap effects on Slender Wing-Body interference. Figure 2b and 2c displays that there are gaps between an all movable wing and the missile like slender body. These gaps resulted in a small reduction in the wing lift. Landahl [5] used a method of matched asymptotic expansion in his research and concluded that a longitudinal gap results in a more substantial reduction in total lift than lateral gaps, Figure 2a. In Reference [6], Abernathy investigated the aerodynamic characteristic of a wing-elevon when an air gap exists between the wing trailing edge and the elevon leading edge. Analytical results were derived from the subsonic kernel function method. Another analytical analysis of gaps was conducted by Ando [7]. He investigated non steady loads on a 2D thin airfoil with a thin narrow gap using Possio's integral equation. A representation of his analysis is depicted in Figure 2d.

Guide projectiles have a gap between the wing and body due to a wing folding mechanism/capabilities. Mikhail in References [8] thru [10] investigated gap effects on guided projectiles. An algebraic model was established, based on wind tunnel data correlation that predicted the normal force losses for fins with large fin-body gaps in transonic and supersonic

speeds. The analysis covers the Mach range 0.8 < M < 4.0 and extends the applicability to both small and large fin gap heights. The models were validated using eighteen cases of wind tunnel tests.

More recent investigations were conducted by Shaojie [11] where he employed 3-D Reynolds-Averaged Navier-Stokes to investigate change is rolling direction of a rocket. The asymmetrical gaps and folding mechanism brought some other disadvantages such as lift coefficient decreasing, drag coefficient increasing and longitudinal static stability margin reduction as shown in Figure 2g.

Gunasekaran [12] performed a wind tunnel experiment to determine the effects of chordwise slots in reducing the wingtip vortex. The balance of induced and parasite drag and the rollup process of wingtip vortex from a NACA 0012 wing was affected by allowing the free stream to pass through chordwise slots connecting the leading and trailing edge of the wing at multiple spanwise locations. It was also disclosed that the Northrop's X-56 experimental plane had chordwise slots at wingtip.

Effect of spanwise trailing edge gaps on aerodynamic performance was reported by Inman [13]. A wind tunnel test was conducted to determine the effects of the trailing edge gaps at high angles of attack, Figure 2e.

2.1.2 Model Description

A simple flat plate swept wing structural model was developed in MSC Nastran. The model was cantilevered at the root. The first three vibratory modes were involved in the flutter mechanism. Figure 3 depicts the first three vibratory modes.

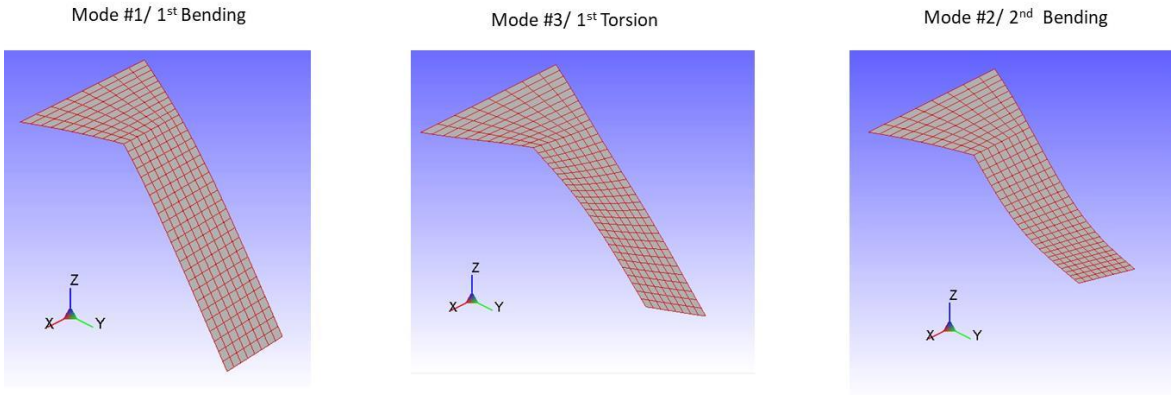

Figure 3. Swept Wing Structural Model – Modes

ZAERO was used to aerodynamically model the wing and to perform both the flutter and gust response analysis. The aerodynamic model had 40 spanwise strips and 10 chordwise boxes for a total of 400 aerodynamic total boxes. The aerodynamic model is reproduced in Figure 4. The

aerodynamic gaps were initially modeled by redefining the aerodynamic panel to generate a physical gap in the wing. This process was very time consuming. The final method was to zero the box pressures that represented the gap for all reduced frequencies. Both chordwise gaps (stream direction) and spanwise gaps were investigated.

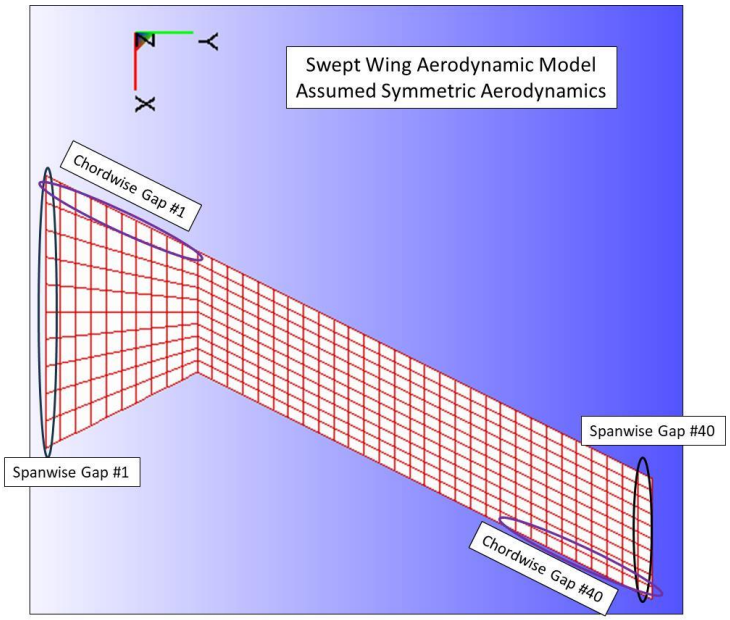

Figure 4. Aerodynamic Box Layout and aerodynamic gap representations

A spanwise gap was assumed to be all the aerodynamic boxes at a constant span location, from the leading edge box to the trailing edge box at the given location. At a constant percent semi-span location all 10 chord box pressure are set to zero pressure to simulate a constant percent semi-span aerodynamic gap. This resulted in a total of 40 span gaps that were analyzed with spanwise gap#1 being located at the root chord and the spanwise gap #40 located at the tip. A chordwise gap was assumed to be at a constant percent chord location, the corresponding 10 spanwise box pressures are set to zero to simulate a constant percent chord aerodynamic gap. This resulted in a total of 40 chordwise cuts that were analyzed. The chordwise boxes were arranged in 4 span locations: inboard (root), inboard middle, outboard middle and outboard (tip). A total of 80 different aerodynamic gaps were modeled and analyzed.

2.1.3 Analysis Procedure

The aerodynamic gaps were originally modeled using the ZAERO CPFACT card which multiplies the computed unsteady aerodynamic pressures by a complex weighting factor. The weighting factor was zero. Examining the resulting pressure plots verified that the box pressures were reduced, but not necessarily set to zero. This nonzero net box pressure was because the interaction of the remaining aerodynamic box pressures on the assigned box results in a non-zero box pressure. Erich Ritz, ZONA Technology Inc., developed a MATLAB script that would take the baseline box Aerodynamic Influence Coefficient (AIC) and zero out the boxes of interest and the interaction of the other boxes on the desired boxes. Thus the “Baseline Model” pressures were written out by ZAERO and the MATLAB scrip was used to zero the box pressures for

every reduced frequency to represent an aerodynamic model of the physical gap. The modified gap AICs were reread into ZAERO and flutter, trim and gust analyses was performed for the respective chordwise or spanwise aero dynamic gap.

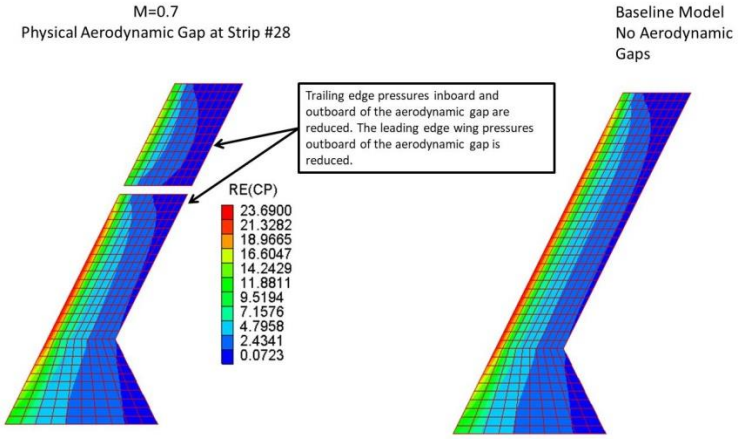

Figure 5. Static Pressure Contours with simulated gap

A comparison of the baseline static pressure coefficients (Cp) contours with the Cp contours calculated for a simulated gap at strip #28 is presented in Figure 5. This verifies that the procedure for zeroing out the boxes for the simulated aerodynamic gap was successful.

2.1.4 Constant Span Aerodynamic Gap Results

As shown in Figure 4 there were forty different constant span aerodynamic gaps that were analyzed with span gap #1 located at the wing root and span gap #40 at located the wing tip. Flutter analysis were conducted using ZAERO with the modified box AIC's for a fixed Sea level density and M=0.7. The change in flutter velocity and flutter frequency compared to baseline results is presented in Figure 6.

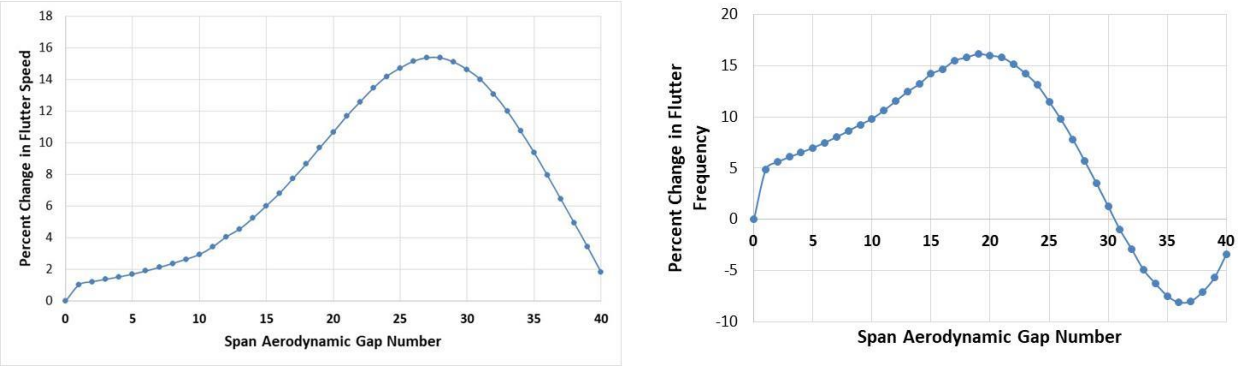

Figure 6. Percent Change in Flutter Velocity and Flutter Frequency for Span Aerodynamic Gaps

The wing flutter speed is increased for each of the forty modeled gaps. The minimum increase in flutter is for an aerodynamic gap at the root (where the aerodynamic load is the highest). It is

observed that the maximum percent increase in flutter speed (15.4%) was located at span identification location #27, which is 68% of the wing semi-span. The span aerodynamic gaps with identification Locations #25 through #30 was the region of maximum flutter speed increase. The aerodynamic gaps in the range of 63% through 75% wing semi-span resulted in the largest increase flutter speed. Generally the flutter frequency was increased for span gaps #1 through #31. From #31 through #40 the flutter frequency was decreased. **It should be noted that the structural model stiffness and mass properties remained constant for this study.**

The resulting V-g-ω plot comparing the baseline results with the change in frequency and damping versus velocity for the largest increase in flutter speed, those of the aerodynamic span gap #27 are compared in Figure 7. The basic 3 mode flutter mechanism is plotted and it is noted that the baseline model changes in modal damping and frequencies are similar to the same three modes for the gap #27 except that the flutter speed was increased and the flutter frequencies were increased. Similar V-g-ω results were observed for all the constant span aerodynamic gaps.

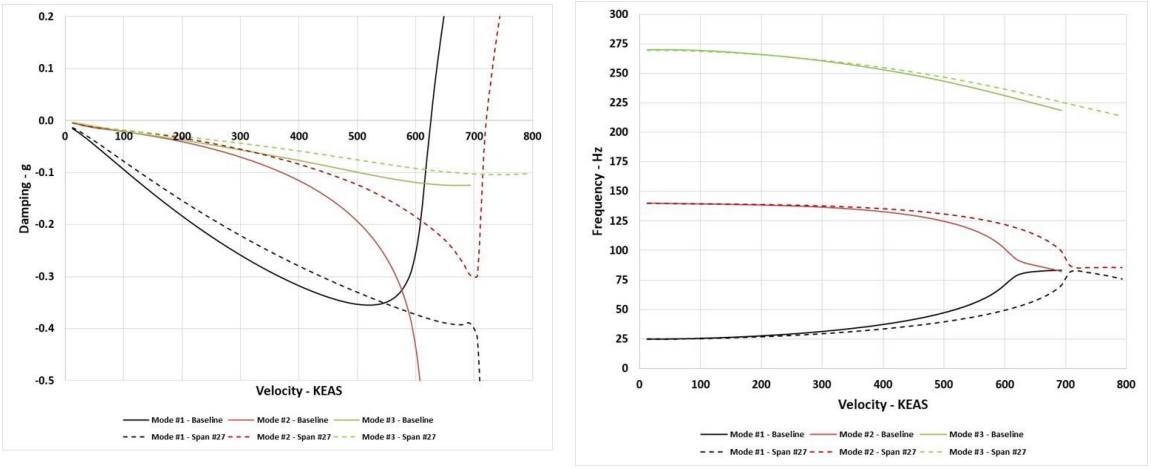

Figure 7. V-g-ω plot Comparison of Baseline with Constant Span #27 Results

An examination of the local spanwise lift and pitching moment was conducted using the ZAERO trim module. The static aerodynamic lift and pitching moment was examined to determine if there was any noticeable correlation between the change in lift and moment that would explain the increase in flutter speed for the constant span aero gaps in the range of 63% through 75% of wing semi-span. Figure 8 is a plot of wing lift and pitching moment calculated for each of the forty span-wise strips. The aerodynamic shear for each of the aerodynamic span strips is shown on the left hand side of Figure 8. The baseline (no aerodynamic gaps) static shear is compared with the static shears for gap #1 (wing root gap), gap #40 (wing tip gap) and gap #27 (gap for maximum increase in flutter speed). The root aerodynamic gap affects the static shear at the root and also has considerable reduction in shear along the semi-span all the way out to gap #32 location. The aerodynamic static shear at tip span (#40) displayed little effect inboard with only a localized reduction near the tip. The span gap #27 had a reduction in shear inboard of the reference strip starting at gap #10. It also had a reduction in shear from gap #27 to gap #37 which was near the tip. The static span moment plot (Figure 8 right side) has similar trends with that

just discussed for the static shear. The shear load and pitching moment was zero at gap #27 and was considerably reduced from the baseline moments from gap #20 thru gap #37.

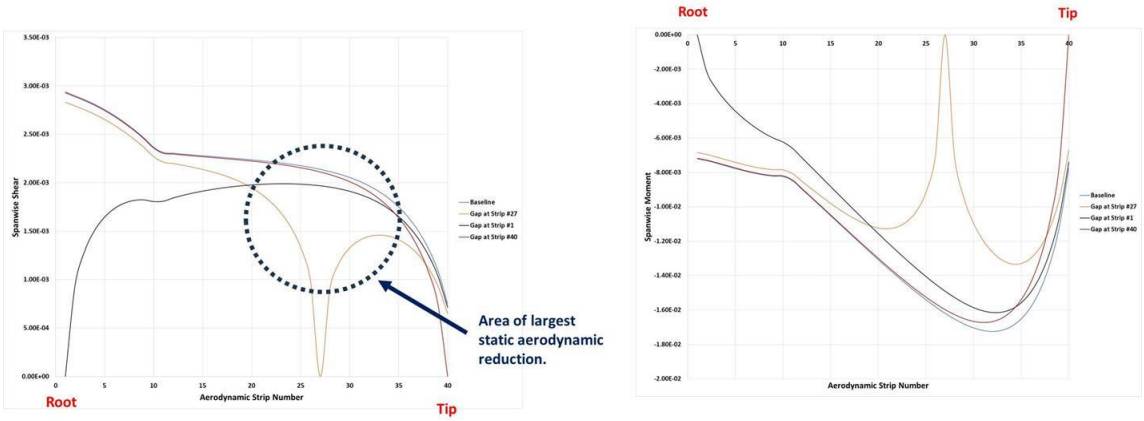

Figure 8. Static Aerodynamic Spanwise Shear and Pitching Moment

The static aerodynamic loads were integrated to determine the total root normal force, the total root torsion and the total root bending moment. The results for the root normal force and root torsion for each of the forty modeled aerodynamic gaps is presented as a percent change compared to the base line results for each of the forty spanwise aerodynamic gaps. Figure 9 presents the percent changes in the static rigid normal force that were observed for each of the forty constant span aerodynamic gaps. The region of largest reduction in lift curve slope is in the region of the inboard wing. Generally, reducing the lift curve slope of a wing will increase the flutter speed of the wing. However, this is not the case for the spanwise gaps, where the largest increase in the flutter speed is located about 60%-75% of the semi-span.

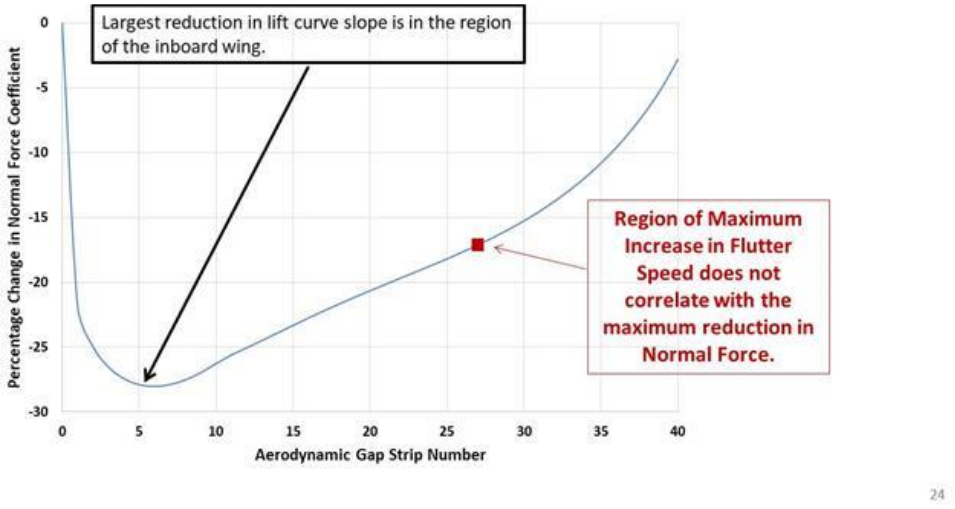

Figure 9. Percent Change in Static (Rigid) Wing Total Normal Force Coefficient Versus Aerodynamic Gap Span Location

The percent change in Static (Rigid) wing root torsion force coefficient versus spanwise aerodynamic gap at each span location is shown if Figure 10. The largest change in torsion was noted at gap number 27. Note that the region of maximum increase in flutter speed does correlates with the area of maximum reduction in torsion as shown by the red square symbol. The horizontal dashed black line displays that the wing root torsion reduction is somewhat flat in the range from 20% to 78% percent wing semi-span.

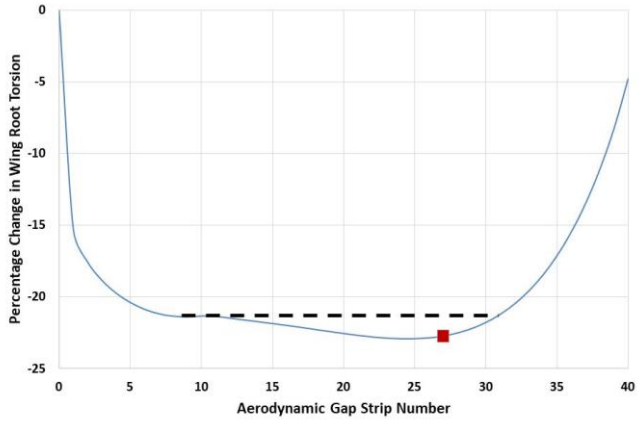

Figure 10. Percent Change in Static (Rigid) Wing Root Torsion Force Coefficient Versus Aerodynamic Gap Span Location

The aerodynamic boxes were integrated to determine the percent change in wing root bending moment for each of the forty spanwise gaps when compared to the baseline value. The resulting wing bending moment is displayed in Figure 11.

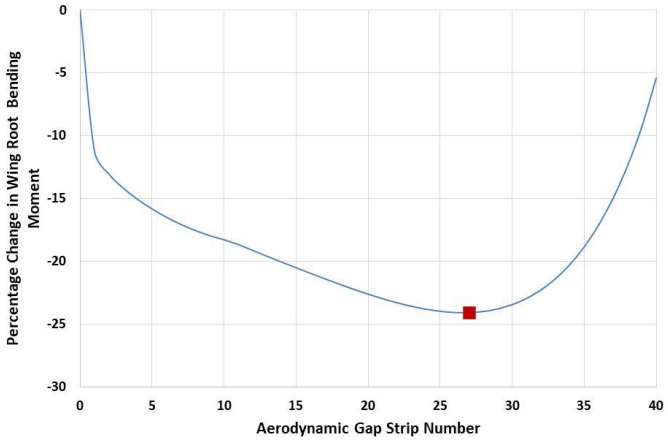

Figure 11. Percent Change in Static (Rigid) Wing Root Bending Moment Coefficient Versus Aerodynamic Gap Span Location

The region of maximum reduction in wing root bending moment is for gap #27 as noted by the red square symbol. Just like the wing root torsion, the region of maximum increase in flutter speed (Figure 6) does correlates with the maximum reduction in wing bending moment, similar to the wing root torsion plot from Figure 10.

The baseline wing sharp edge gust response was evaluated at Mach = 0.7 and Sea Level and compared with the responses for each of the 40 spanwise aerodynamic gaps. The wing root flexible shear and torsion response is plotted in figure 11 as a percent reduction over the base line sharp edge gust flexible response.

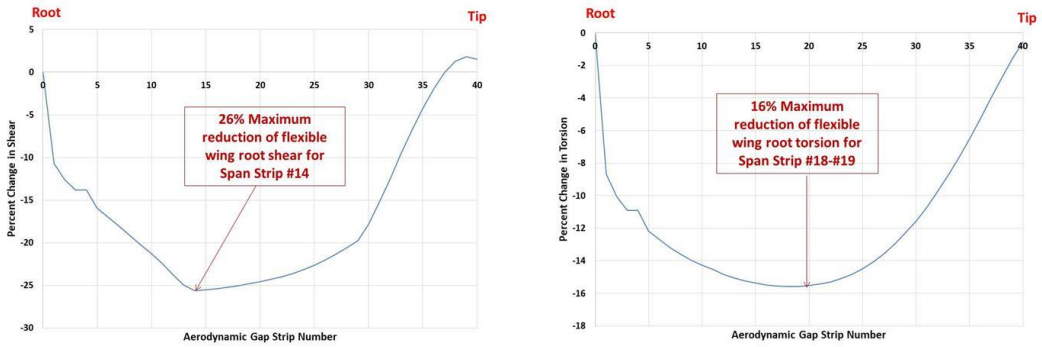

Figure 11. Sharp Edge Gust Percent Change in Flexible Wing Root Shear and Torsion versus Aerodynamic Gap Span Location

It was noted that the gaps that resulted in the maximum change in the flexible wing root shear was more inboard (Span gap #24) than the gaps that resulted in the maximum increase in flutter speed. The maximum reduction in the flexible wing root shear was 26 percent. The maximum reduction in flexible wing root torsion was for gaps #18 and #19 that resulted in a 16 percent reduction in the flexible wing root torsion. The aerodynamic gap for maximum wing root torsion reduction was more outboard than that for maximum wing shear reduction. The sharp edge gust response wing percent change for flexible wing bending moment and wing tip deflection for the forty modeled spanwise aerodynamic gaps is presented in Figure 12. The percent change in bending moment versus aerodynamic gap is presented on left side of Figure 12. There is a fifteen percent reduction in the bending moment for gaps fifteen through nineteen, which is mid wing semi-span. The wing tip displacements that resulted from the sharp edge gust for the various gaps were monitored and are plotted on the right side of Figure 12. The maximum reduction of flexible wing tip deflection was found to be twenty-nine percent for span gaps # 22 and # 23. The sharp edge gust wing response to spanwise aerodynamic gaps is significantly different from the flutter response for the same gaps. Where the aerodynamic gap located inboard at station fourteen is the location of maximum flexible shear reduction. The mid span gaps resulted in the sharp edge gust maximum reduction for flexible wing root torsion and bending moment. The outboard gaps, twenty-two and twenty-three, resulted in the maximum wing tip deflection reduction.

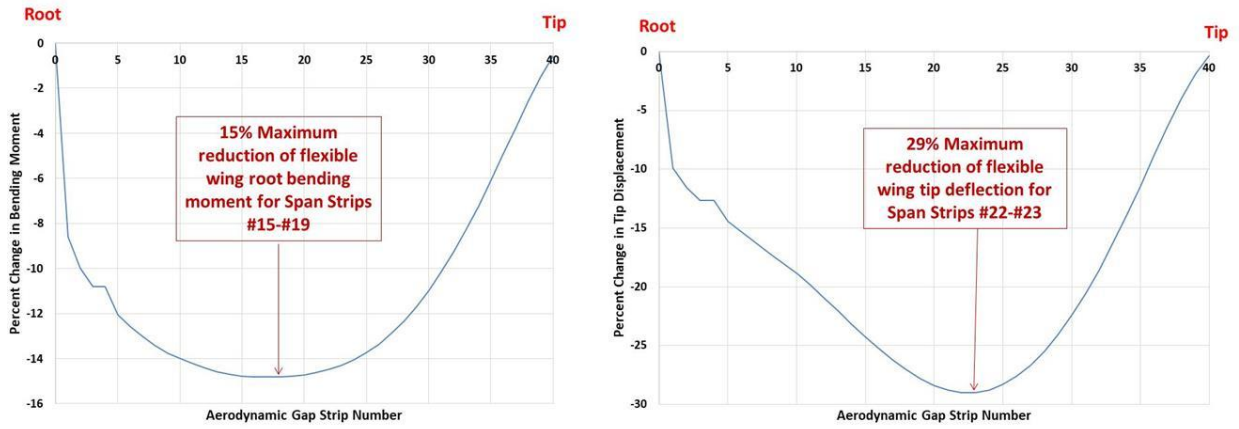

Figure 12. Sharp Edge Gust Percent Change in Flexible Wing Root Bending Moment and Wing Tip Deflection versus Aerodynamic Gap Span Location

A summary of the time history response for the sharp edge gust for a spanwise aerodynamic gap at station fourteen (location for maximum of wing root shear) is presented in Figure 13. The figure compares the time history response of the baseline wing flexible: root shear, root bending moment, root torsion and tip deflection with the corresponding response of the wing with an aerodynamic gap at station fourteen.

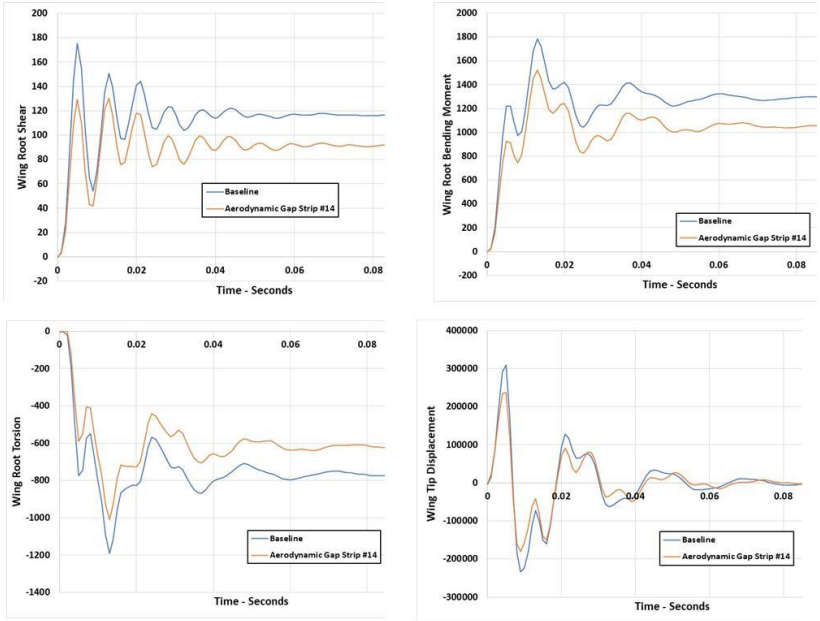

Figure 13. Sharp Edge Gust Response for a Spanwise Aerodynamic Gap at Span Station Fourteen

The time history plots, for a time length of 0.08 seconds, displays a reduction in flexible wing root shear, torsion, bending moment and tip deflection for an aerodynamic span gap at span station number fourteen. The figure displays a reduction in all the gust loads over the time history response. It is also noted that the relative peaks and valleys appear at roughly the same time; meaning that the gust response frequency doesn't change.

Figure 14 summarizes the spanwise location of aerodynamic gaps that resulted in maximum increase in flutter speed and maximum reduction in the gust flexible wing root shear. The aerodynamic gaps at a constant span location from leading edge to trailing edge resulted in a 15.4 percent increase in flutter speed over the baseline wing for gap # 27 of the forty modeled gaps. Interestingly, the constant spanwise aerodynamic gaps for maximum reduction of the flexible wing root response was significantly inboard of the spanwise gap for maximum response for flutter speed increase.

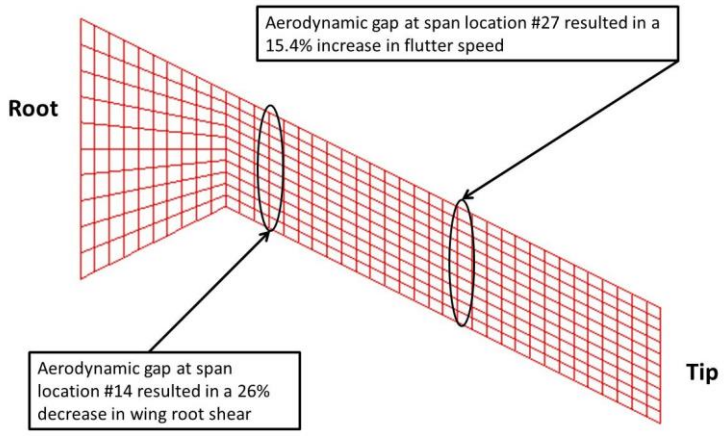

Figure 14. Spanwise location of Aerodynamic Gaps that Resulted in Maximum Increase in Flutter Speed and Maximum Reduction in Gust Flexible Wing Root Shear

2.1.5 Constant Span Aerodynamic Gap Results

A second set of aerodynamic gaps were considered in this investigation as shown in Figure 15. These gaps were considered to be at a constant percent chord cut. Each chordwise gap had ten aerodynamic boxes located at same the percent relative wing chord location in the spanwise direction. The wing was divided into four reference span locations with each reference span location having ten chord cuts. The wing was divided into four spanwise locations with each having ten chord wise aerodynamic gaps as displayed in Figure 15. This resulted in a total of forty constant chord aerodynamic gaps.

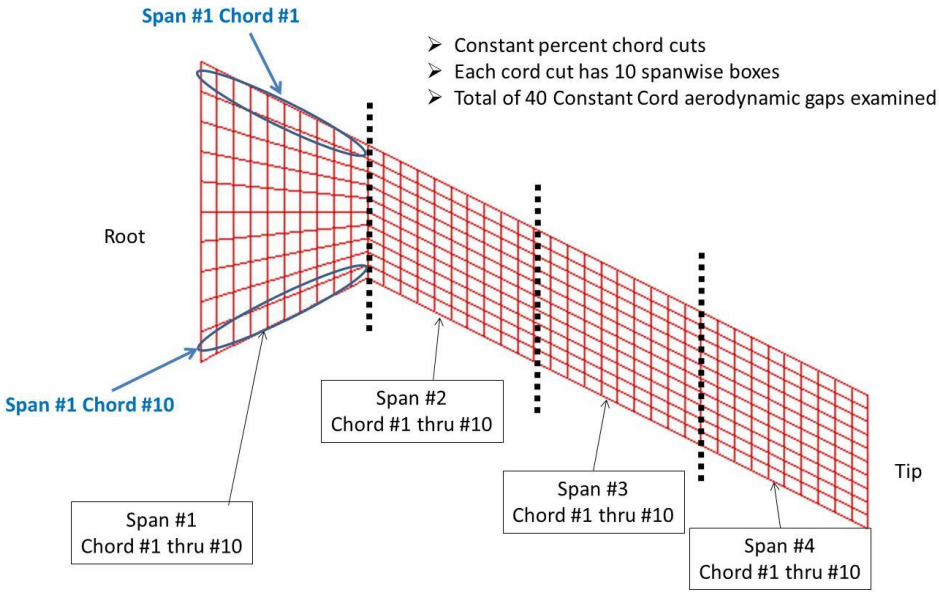

Figure 15. Layout of Simulated Constant Chord Aerodynamic Gaps

Similar to the constant spanwise aerodynamic gaps reported in section 2.1.4, flutter, static trim and gust analysis were conducted for each of the forty constant chord aerodynamic gaps. Flutter analyses were conducted at Mach=0.7 Sea Level for the baseline wing with no aerodynamic gaps and the resulting flutter speed and flutter frequencies were compared with those found with the constant chord aerodynamic gaps. The flutter speeds are reported in Figure 16. For ease of the ten modeled constant chord aero gaps results for each of the four span groups are presented.

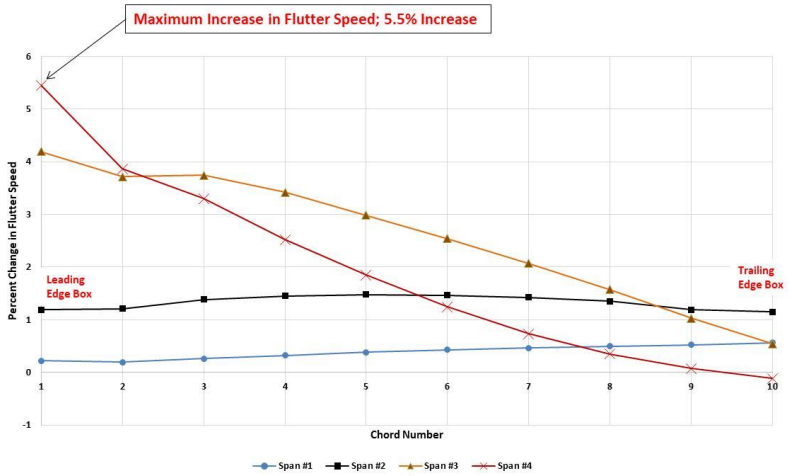

Figure 16. Percent Change in Flutter Speed for Constant Chord Aerodynamic Gaps, Summarized for each of the Four Span Stations

The percent change in flutter speed is plotted on the vertical axis and the horizontal axis plots the results identifying for each of the four constant span aerodynamic gap location the leading edge location (chord number 1) to the trailing edge location (chord number 10). The blue line is the most inboard span station. This location resulted is the smallest increase in flutter speed (less than 1 percent) for all constant chord aerodynamic gaps. The results for span location # 3 and # 4 display that the aerodynamic gaps at the leading edge of the wing resulted in the larger percent increase in flutter speed when compared to the trailing edge gaps. The maximum increase in flutter speed of 5.5 percent was for the gap at the leading edge outboard span location.

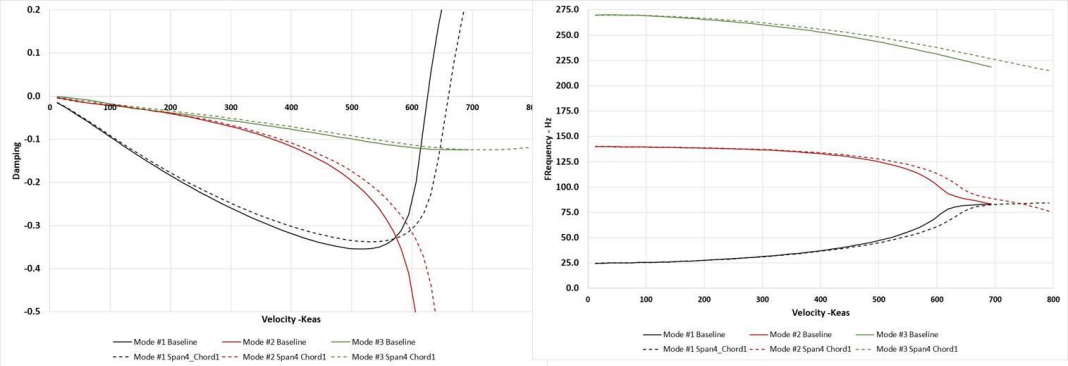

Figure 17. V-g-ω Plot Comparing Baseline Results with those of the Span #4 Chord #1 Constant Chord Aerodynamic Gap

The baseline three mode flutter mechanism V-g-ω plot is compared to the results for the case that resulted in the maximum increase in flutter speed for the constant cord gap. The aerodynamic doesn't change the flutter mechanism; it just provided a 5.5 percent increase in flutter speed.

Static trim analyses were conducted to determine the effects of the chordwise gaps on the overall wing aerodynamic normal force and pitching moment. A comparison of the baseline normal force (blue line) and the pitching moment (blue line) is compared to the corresponding values of the constant chordwise gap at the leading edge of span station number 4 (red lines) is shown in Figure 18. The normal force (left side Figure 18) displays no difference inboard of fifty percent semi-span location. For the fifty percent semi-span location there is a slight change in normal force with essentially no difference at the tip. The pitching moment (right side of Figure 18) displays a reduction (red line) for the aerodynamic gap for fifty percent semi-span to seventy percent semi-span. The pitching moment for the two cases are the essentially the same at the wing tip.

As mentioned previously in Section 2.1.4 the spanwise static loads were monitored for each modeled aerodynamic gap to determine if there was any correlation between the local

aerodynamic load and the resulting increase in flutter speed and decrease in the sharp edge gust response.

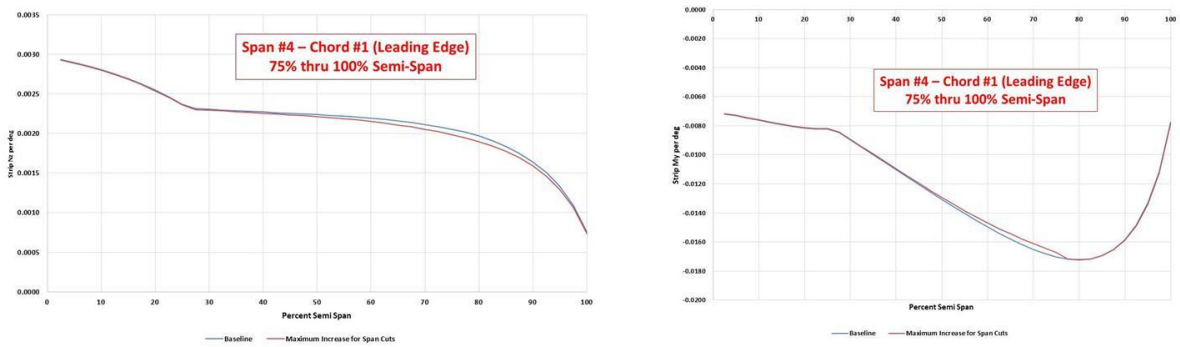

Figure 18. Spanwise Normal Force and Pitching Moment Comparison for Constant Chord Gap at Span Station #4 (most outboard span location)

The static aerodynamic forces were integrated to determine the wing normal force for the forty constant chord aerodynamics. The percent change in the wing normal force is plotted on the horizontal axis of Figure 19 with the percent change in flutter speed plotted on the vertical axis.

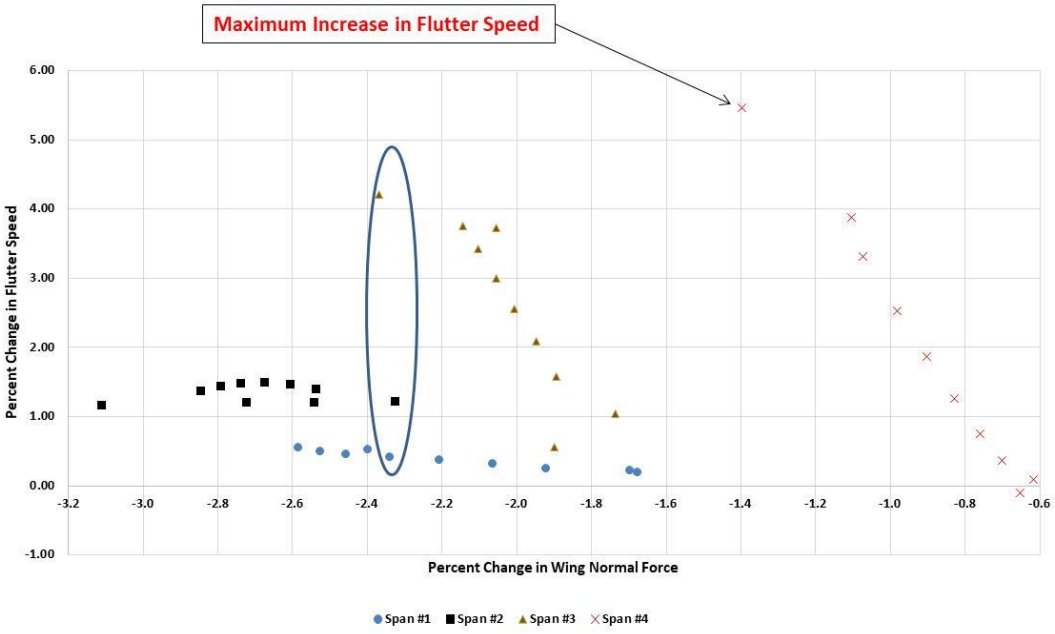

Figure 19. Percent Change in Flutter Speed versus Percent Change in Wing Static Normal Force

It is noted in Figure 19 that the maximum percent decrease in the wing static normal force is of the order of -3.2 percent for the span location number two (square symbols) but this reduction in normal force only resulted in an increase in flutter speed of a little over one percent. There are ten symbols for each span location that vary from the leading edge to the trailing edge as shown in Figure 15. For the chordwise aerodynamic gaps there are regions with the same percent change in wing normal force that result in different increases in flutter speed. One such instance is highlighted in Figure 19 by the blue oval. The maximum increase in flutter speed occurred for the leading edge constant chord gap for span station number 4. This resulted in a 5.5 percent increase in flutter speed with a corresponding decrease in wing normal force of only -1.4 percent. The maximum decrease in the wing static normal force does not result in the maximum increase in flutter speed.

A plot of percent change in flutter Speed versus the percent change in the static wing pitching moment for the constant percent chord gaps for the four span locations is displayed in Figure 20.

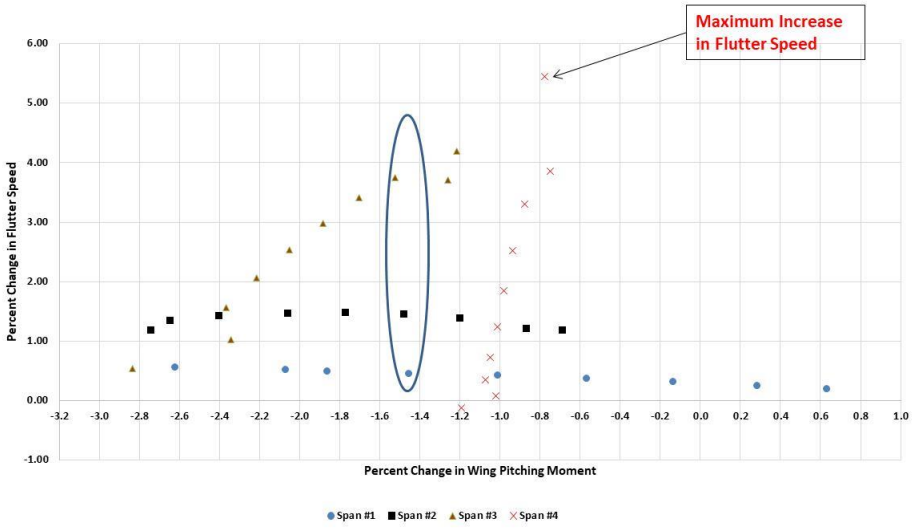

Figure 20. Percent Change in Flutter Speed versus Percent Change in Wing Static Pitching Moment

The maximum percent change in the wing static pitching moment was accomplished for span location number three. The maximum change in pitching moment resulted in a mere 0.5 percent increase in flutter speed. Similar to as noted for Figure 19 there are numerous instances of the same percent change in pitching moment that resulted in different flutter speeds. The maximum increase in flutter speed was for the constant chord gap at the leading edge of span location. It is interesting that some of the aerodynamic gaps for span location number one (blue circles) that resulted in an increase the pitching moment.

A plot of percent change in flutter speed versus the percent change in the static wing bending moment for the constant percent chord gaps for the four span locations is shown in Figure 21.

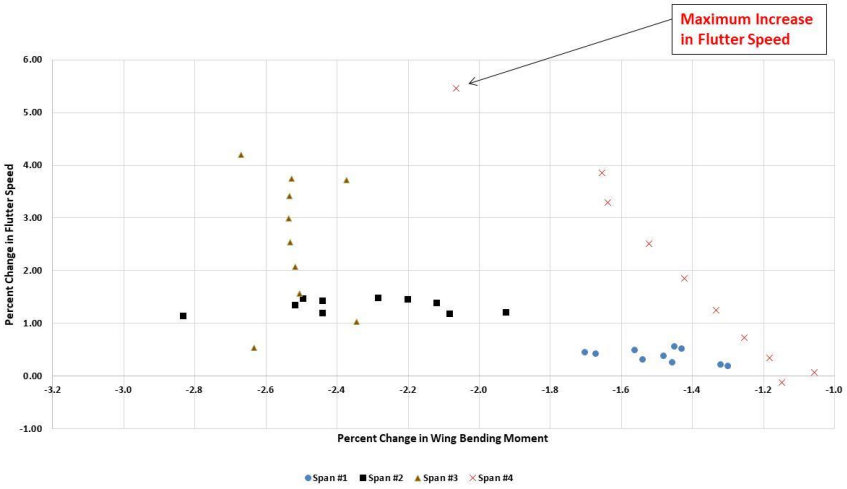

Figure 21. Percent Change in Flutter Speed versus Percent Change in Wing Static Bending Moment

The maximum percent change in the wing static bending moment (-2.82 %) was accomplished for span location number two (black square symbol). This gap location resulted in a 1.25 percent increase in flutter speed. There are numerous instances of the same percent change in bending moment that resulted in different flutter speeds for different constant chord aerodynamic gaps at different span locations. The maximum increase in flutter speed was for the leading edge constant chord box gaps for span location number 4. This results in a 5.5 percent increase in flutter speed that resulted in a decrease in the static bending moment decrease of 2.05 percent.

The wings with the forty constant chord aerodynamic gaps was subjected to a sharp edge gust for the flight condition Mach=0.7 Sea Level altitude and the flexible wing root shear, torsion, bending moment and tip deflection were obtained from the time history response. Figure 22 presents a summary of the percentage change in wing flexible root shear compared to the baseline for the constant chordwise aerodynamic gaps for each of the four spanwise locations. The horizontal axis reflects the relative chordwise location of the aerodynamic gaps (#1 is the leading edge boxes and #10 represents the trailing edge aerodynamic boxes). The gaps at span location number 1 (inboard root location – blue circles) resulted in roughly a 2 percent reduction in the sharp edge gust root shear response. The reduction for this location is flat from the leading edge to the trailing edge. The gaps at span location number 2 (black squares) resulted in roughly a 4 percent reduction in the sharp edge gust root shear response. Similar to span location 1, the reduction in shear force for span location number 2 is flat from the leading edge to the trailing edge. The constant chord gaps for span location 3 and 4 show a trend of an increased reduction in wing shear progressing from the trailing edge to the leading edge. Examining Figure 22

verifies that the maximum decrease in the root shear gust response of 7.4 percent was at span location number 3 and constant chord location number 1 was. A nearly identical reduction was achieved by a gap at span location number 4 and constant chord location number 1 with a reduction of 7.4 percent.

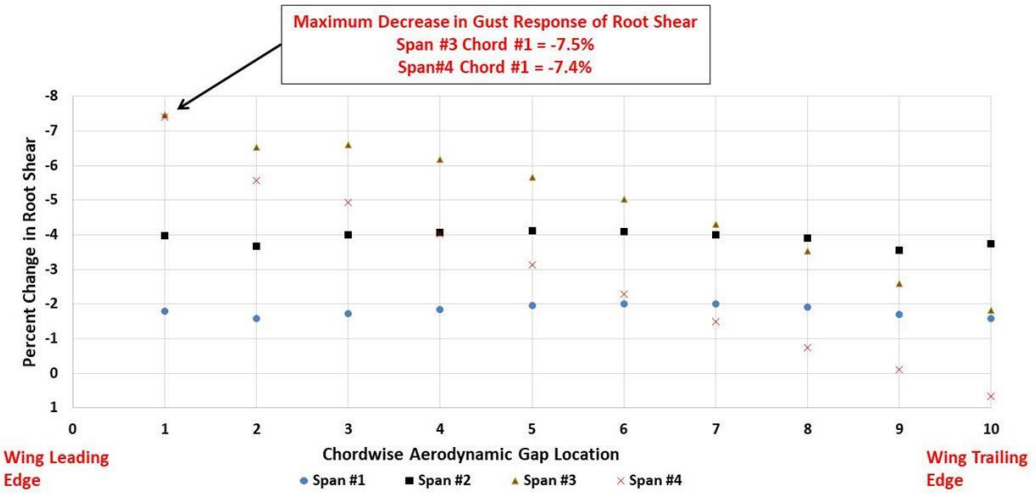

Figure 22. Percentage Change in Wing Flexible Root Shear Gust Response Compared to the Baseline for the Constant Chordwise Aerodynamic Gaps

The maximum reduction in wing root torsion as identified from the sharp edge gust time history response for the forty constant chord gaps is shown in Figure 23.

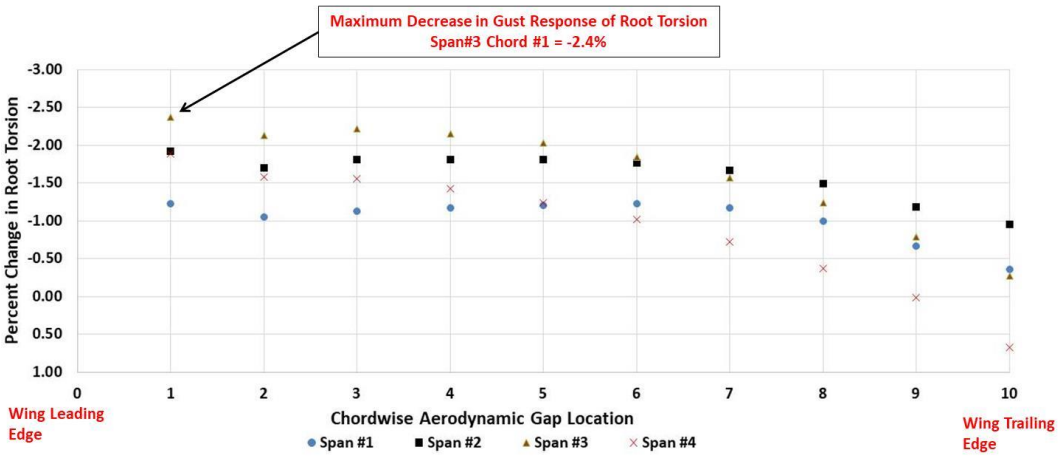

Figure 23. Percentage Change in Wing Flexible Root Shear Gust Response Compared to the Baseline for the Constant Chordwise Aerodynamic Gaps

The maximum percent reduction in wing root torsion of 2.4 percent for span location number three for the constant chord gap at the leading edge or chord identification number 1. The constant chord gaps for span station number one and two displays a flat variation in the reduction from the leading edge to the trailing edge. The most outboard tip span location, number four, corresponding reduction in wing root torsion was overall less effective than that noticed for span number three.

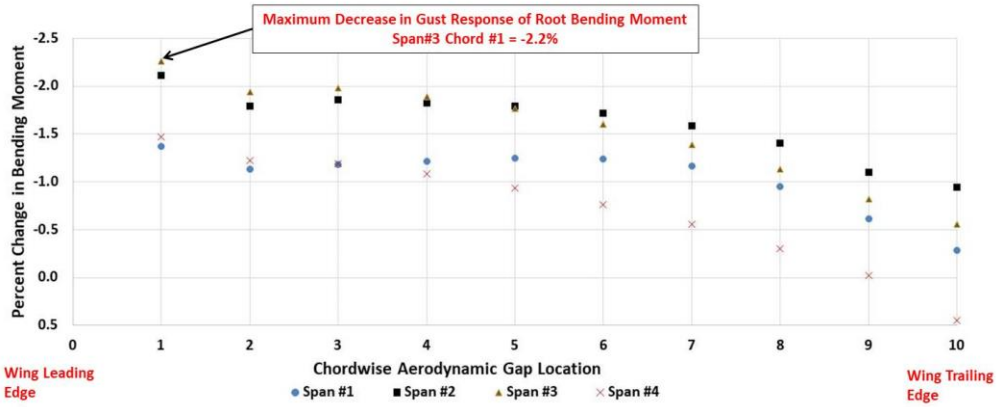

Figure 24. Percentage Change in Wing Flexible Root Bending Moment Gust Response Compared to the Baseline for the Constant Chordwise Aerodynamic Gaps

The sharp edge gust time history response for the sample wing, with and without constant chord aerodynamic gaps, was monitored to determine the percent change in flexible wing bending moment for the forty gaps. The maximum percent change in gust response of the root bending moment was for span location number three for constant chord location at the wing leading edge, chord Identification number one. The reduction was 2.2 percent over the baseline flexible wing root bending moment.

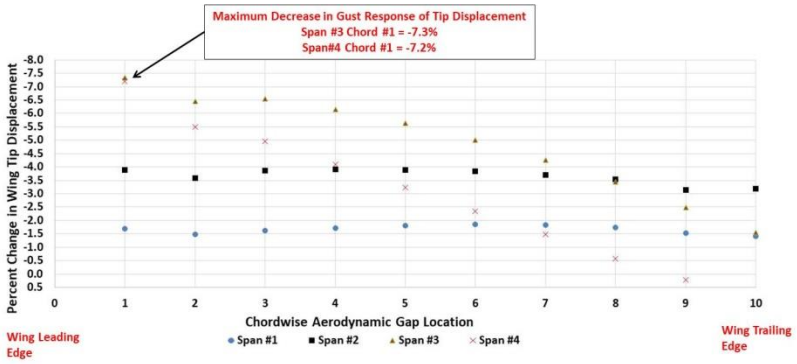

Figure 25. Percentage Change in Wing Tip Deflection Gust Response Compared to the Baseline for the Constant Chordwise Aerodynamic Gaps

The wing tip response maximum time history response for the sharp edge gut is plotted in Figure 25. The maximum decrease in of the tip displacement was at the leading edge for both span location and location 4. The reduction was 7.3 percent for span location three and 7.2 percent for span four. The reduction tip deflection for span locations one and two were invariant for the gaps transiting from the leading edge to the trailing edge.

A summary of the time history response for the sharp edge gust for constant chordwise aerodynamic gaps for the case that resulted in the largest reduction in gust response is reproduced in Figure 26. The figure compares the time history response of the baseline wing flexible: root shear, root bending moment, and root torsion. The plotted response is for a constant chordwise gap at cord identification number one (leading edge) and span location number three.

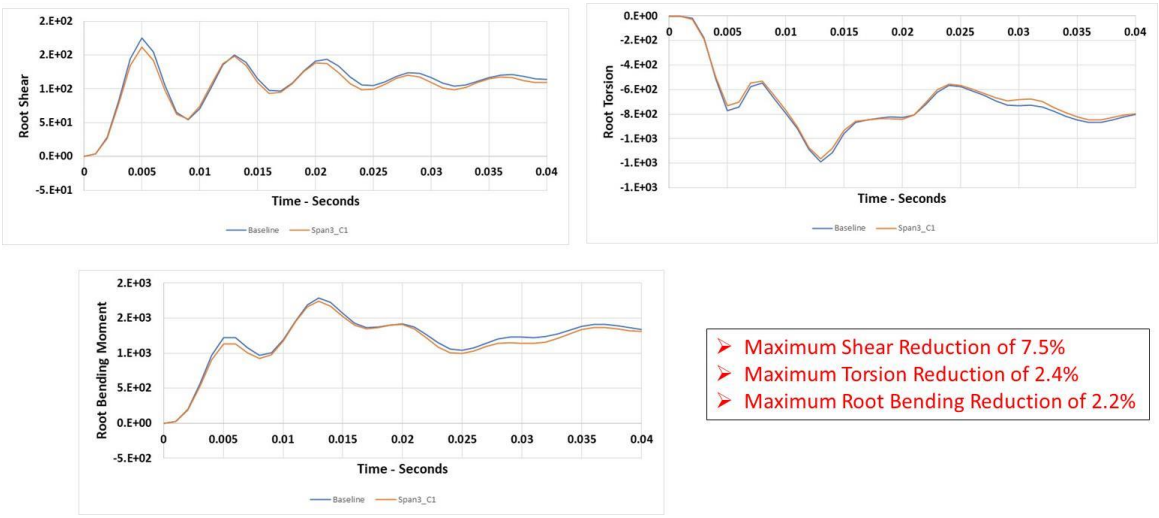

Figure 26. Sharp Edge Gust Response for a Chordwise Aerodynamic Gap at Span Location 3 and Chordwise Identification 1

The time history plot for a time length of 0.08 seconds displays a reduction in flexible wing root shear of 7.5 percent, torsion of 2.4 percent and 2.2 percent of wing root bending moment. The figure displays a reduction in all the gust loads over the time history response. It is also noted that the relative peaks and valleys appear at roughly the same time; meaning that the gust response frequency doesn't change.

3 CONCLUSIONS

An investigation of a simple swept wing with simulated aerodynamics gaps in the wing was conducted for aerodynamic gaps. The first set of gaps examined were at a constant span location with the ten corresponding aerodynamic box pressures from the leading edge box to the trailing edge box set to zero pressures. There were forty spanwise gaps that transitioned from the root to

the tip were analyzed for flutter and gust response. The second set of gaps was for boxes that were at a constant percent chord cuts. There were ten chord boxes at each percent chord that were examined from the wing leading edge to the wing trailing edge at four span locations that transitioned from the wing root to the wing tip,. There were a total of forty constant chord gaps considered. A summary of the spanwise and constant chord aerodynamic gaps that resulted in the biggest increased in the flutter speed and reduction of the gust response is shown in Figure 27.

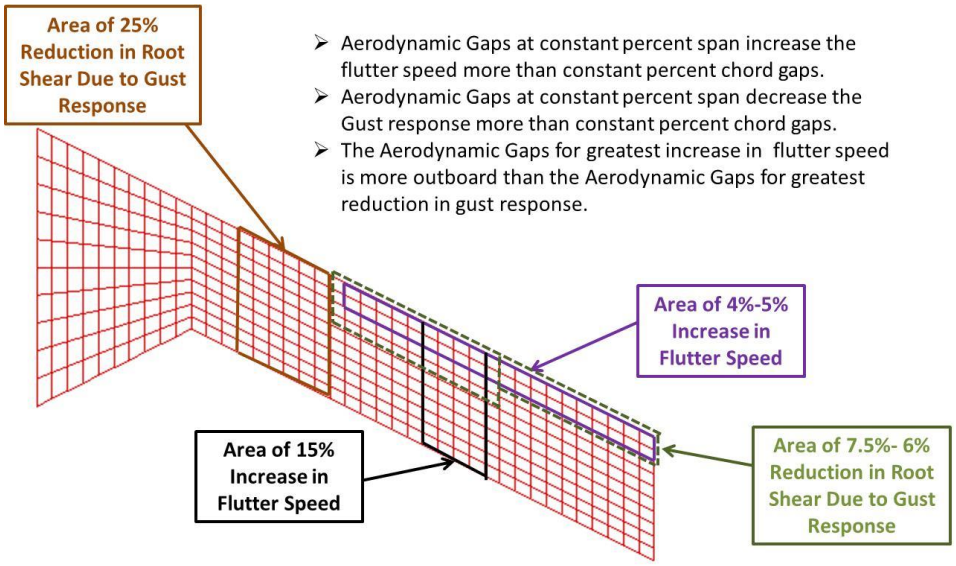

Figure 27. Location Summary of Maximum Flutter Speed Increase and Maximum Reduction in Gust Response.

The aerodynamic gaps at constant percent span were found to increase the flutter speed more than constant percent chord gaps. The aerodynamic gaps at constant percent span were found to decrease the gust response more than constant percent chord gaps. Interestingly, the aerodynamic gaps for greatest increase in flutter speed were more outboard than the aerodynamic gaps that resulted in the greatest reduction in gust response. The maximum increase in flutter speed for spanwise aerodynamic gaps appeared to match the condition when the gap was in the region of seventy percent semi-span of the wing. Additionally, the aerodynamic gaps located near the leading edge resulted in largest increases in flutter speed. The best aerodynamic gap location to minimize gust response was not at the same location as the best aerodynamic gap location to increase flutter speed. The best aerodynamic gap location to minimize gust response was inboard of the seventy percent semi-span location of the wing.

The static aerodynamic monitoring of the spanwise aerodynamic loads did not show correlation of the aerodynamic gaps effects on the maximum lift and pitching moment reductions with a relative increase in flutter speed or relative decrease in the sharp edge gust response.

In reference [14] Fung states: “Application of the Two-Dimensional Analysis. Regarding the two dimensional airfoil as a typical section of a three-dimensional wing, and adjusting the spring constants in such a way that the frequencies ω_h, ω_α, etc., coincide with the actual uncoupled free vibration frequencies of the wing, while the mass and geometric properties are taken as those of a typical section, one may expect that the critical flutter speed calculated for the two-dimensional case approximates that of the actual wing. This was shown to be true by Theodorsen and Garrick for wings without appreciable sweep angle, without large concentrated mass, with more or less uniform distribution of structural properties across the span, with straight elastic and inertial axes, and with high chordwise rigidity. **The location of the typical section is of some importance. Generally it is taken in the neighborhood of 0.7 span from the root, or at the mid-span of the aileron.”**

Interestingly, this investigation confirmed this representation of the Two-Dimensional Analysis as the location of the maximum generalized aerodynamic forces and the aerodynamic gaps maximized location. The maximum increase in flutter speed for aerodynamic gaps appeared to match the condition when the gap was in the region of 0.7 semi-span of the wing from the root. The aerodynamic Gaps located near the leading edge resulted in largest increases in flutter speed. The best aerodynamic gap location to minimize gust response was not at the same location as the best aerodynamic gap location to increase flutter speed. The best aerodynamic gap location to minimize gust response is inboard of the 0.7 span locations from the root.

REFERENCES

[1] Pendleton, E., Lee, M., Wasserman, L., A Low Speed Flexible Model Simulating an F-16 Derivative Wing Design, WRDC-TR-90-3083, Jan 1991.

[2] Mirels, H., Gap Effect on Slender Wing-Body Interference, *Journal of the Aeronautical Sciences*, Vol. 20, Issue 8, 1953.

[3] Bleviss, Z., Some Aerodynamic Effects of Streamwise Gaps in Low Aspect Ratio Lifting Surfaces at Supersonic Speeds, *Journal of the Aeronautical Sciences*, Vol. 21, Issue 10, 1954.

[4] Dugan, W. D. Hikido, K. Theoretical Investigation of the Effects Upon Lift of a Gap Between Wing and Body of a Slender Wing-Body Combination, NACA TN 3224, 1954.

[5] White, R. B., Landahl, M. T., Effect of Gaps on the Loading Distribution of Planar Lifting Surfaces, *AIAA Journal*, Vol. 6, Issue4., 1968.

[6] Abernathy, J.M., An Analysis of Gap Effects on Wing-Elevon Aerodynamic Characteristics, AIAA 19th Aerospace Science Meeting, AIAA-81-0364, Jan 1981.

[7] Ando, S. and Lee, DH, Unsteady Incompressible Inviscid Aerodynamics of a Thin Airfoil with Narrow Gaps, *AIAA Journal*, Vol. 20 No. 1, 1982.

[8] Mikhail, A.G., Fin Gaps and Body Slots of Guided Projectiles: Effects, Data Correlation and Modeling, Technical Report BRL-TR-2808, 1987.

[9] Mikhail, A.G., Fin Gaps and Body Slots for Guided Projectiles, 25th AIAA Aerospace Science Meeting, Jan 1987.

[10] Mikhail, A.G., Lift Loses for Fin-Body Gaps in Transonic and Supersonic Speeds: Data Correlation and Modeling, AIA-89-0332, 27th AIAA Aerospace Science Meeting, Jan 1989.

[11] Shaojie, G., Zhongyan, Y. , Bin, W. and Peipei, Z., Numerical Investigation for the Effects of Gaps and Folding Mechanism on Aerodynamic Characteristics of a Rocket, 21st AIAA International Space Planes and Hypersonics Technology Conference, Xiamen, China, March 2017.

[12] Gunasekaran, S., and Gerham, T., Effect of Chordwise Slots on Aerodynamic Efficiency and Wingtip Vortex, *AIAA Journal*, Vol. 56, No 12., 2018.

[13] Inman, D. and Sigrest, P., Effect of Spanwise Trailing Edge Gaps on Aerodynamic Performance, AIAA SciTech Forum, Jan 2020.

[14] Fung, Y.C., *An Introduction To The Theory of Aeroelasticity*, Dover Publication, Inc. 1969, Pg. 235.

COPYRIGHT STATEMENT